Lattice Dynamics of a Rigid-Ion Model for Gadolinium Molybdate*

L. L. Boyer† and J. R. Hardy
Behlen Laboratory of Physics, University of Nebraska, Lincoln, Nebraska 68508
(Received 11 December 1972)

Results of lattice-dynamical calculations are presented which support the view that the ferroelectric phase transition in gadolinium molybdate (GMO) arises from the softening and ultimate instability of a doubly degenerate zone-edge mode of the high-temperature paraelectric phase. We have used a rigid-ion model in which the short-range force constants are obtained from a detailed knowledge of the crystal structure together with the conditions imposed by the requirement that the crystal must be in static equilibrium under the combined influence of both Coulomb and short-range forces. Our results show that this type of approach is very useful when one is dealing with complex structures such as GMO, which has thirty-four ions per unit cell in the paraelectric phase. In view of the simplicity of our model we are able to obtain a surprisingly good correlation with experimental results. In particular, our calculated zone-center frequencies reproduce the basic features of the observed Raman spectrum. Dispersion curves are presented which show a pronounced softening of two phonon branches which become doubly degenerate at the M point. This result is in agreement with the results obtained by inelastic neutron scattering. The displacements associated with the soft M-point modes correlate with the difference in the structures of the high- and low-temperature phases determined by x-ray diffraction. This provides further evidence that the ferroelectric domains in GMO are to be interpreted as "frozen-in" soft zone-boundary modes of the paraelectric phase.

I. INTRODUCTION

Gadolinium molybdate [$Gd_2(MoO_4)_3$ or GMO] was found to undergo a ferroelectric transition at 159 °C by Borchardt and Bierstedt.[1] Subsequent studies of this transition by a number of workers have shown that it possesses some very unusual properties. Particularly remarkable is the essential absence of any dielectric anomaly. The clamped dielectric constant shows no temperature dependence while the free crystal exhibits only a small peak at the transition temperature.[2] At the same time, there is a large anomalous elastic behavior which occurs for temperatures $T < 159$ °C. However, this anomaly, as does the peak in the free dielectric constant, vanishes suddenly when $T \geq 159$ °C.[2,3]

Detailed x-ray analyses of the structure of ferroelectric (f.e.) phase of GMO have been performed by Keve *et al.*[4] and Jeitschko,[5,6] while Jeitschko has also made similar studies on the paraelectric (p.e.) phase.[6] The transition is accompanied by a structural change from $P\bar{4}2_1m$ with two formula units per unit cell for p.e. GMO, to $Pba2$ with four formula units per unit cell for f.e. GMO.

The fundamentally new aspect of this transition is that the instability in the p.e. phase results from a softening of a doubly degenerate phonon mode at the zone boundary. This was suggested independently by Pytte,[7] Levanyuk and Sannikov,[8] and Aizu,[9] who observed that such a soft M-point mode would account for the observed doubling of the unit cell. Subsequent neutron-scattering measurements of Axe *et al.*[10] and Dorner *et al.*[11] have shown that this is indeed the case. In the latter paper,[11] dynamical structure analysis was used to examine the relative magnitudes of those eigenvector components which are not fixed by symmetry alone.[12] In this way a linear combination of eigenvectors for the degenerate M-point modes was determined and it was found that the associated displacements could describe the differences between the structures of the two phases.

These authors were also able to explain the appearance of polarization in terms of an order parameter which is proportional to the soft-mode amplitude and which is anharmonically coupled to the macroscopic strain. Since the crystal is piezoelectric, this in turn produces a spontaneous polarization.

The anharmonically induced strain due to a specific soft mode depends upon the "direction" of the mode in the degenerate "plane" of the two soft-mode eigenvectors. From Eqs. (13) and (11c) of Ref. 11, the strain is proportional to $g_{66,1}\sin2\phi + g_{66,2}\cos2\phi$, where ϕ is a rotation in the degenerate "plane" and $g_{66,1}$ and $g_{66,2}$ are coefficients which describe the anharmonic coupling. If we replace ϕ by $\phi + \frac{1}{2}\pi$ this evidently changes the sign of the strain, and thus, domains of opposite strain (polarization) in the f.e. phase must correspond to orthogonal eigenvectors of the degenerate soft modes in the p.e. phase. This point was first discussed by Axe *et al.*[10] However, the subsequent discussion in Ref. 11 is somewhat obscure on this point since it appears that setting $\phi = 0$ and fitting Jeitschko's data for one polarization do not allow for switching.

We have also found that this type of ϕ dependence

in the strain (polarization) is necessary to account for the observed differences between the f.e. and p.e. structures. Furthermore, we conclude that as the transition occurs the crystal "selects" a *particular set* of orthogonal eigenvectors from the degenerate "plane" and the displacements associated with these special eigenvectors are "frozen" into the structure. Again, this is not immediately clear from the discussion in Ref. 11 because of the assumption that $\phi = 0$. However, if the form of the free energy given by Eq. (14) of Ref. 11 is retained then the coefficients of the fourth- and sixth-order terms are functions of ϕ such that they are invariant if ϕ is replaced by $(\phi + \frac{1}{2}\pi)$. A particular set of orthogonal eigenvectors for which the associated displacements become one of the four observed ferroelectric domains is given by $\phi = \phi_m$, where ϕ_m is the value of ϕ (at the transition temperature) for which the free energy is a minimum. The four domain structures thus correspond to ϕ_m, $\phi_m + \frac{1}{2}\pi$, $\phi_m + \pi$, and $\phi_m + \frac{3}{2}\pi$. For $\phi = \phi_m$ or $\phi_m + \pi$ the domains have polarity (strain) $+P_z(+u_{xy})$ and the $\phi_m + \frac{1}{2}\pi$ and $\phi_m + \frac{3}{2}\pi$ domains have polarity (strain) $-P_z(-u_{xy})$. These possibilities account for the unusual switching mechanism in GMO and lead one to consider the possibility of domain walls between regions of like polarity.[13]

Our calculations are based on a rigid-ion model in which short-range interactions between the gadolinium ions and their seven nearest-neighbor oxygen ions are included and similar interactions between the molybdenum ions and their four nearest-neighbor oxygen ions are also taken into account. Our approach requires a detailed knowledge of the crystal structure. Given this and the magnitudes of the ionic charges, we obtain certain equilibrium conditions, which specify the first derivatives of the short-range potentials. Three other parameters (two of which are second derivatives of the short-range potentials and the third of which measures the ionicity of the molybdate group) are obtained by a partial fitting to the observed Raman spectra.

In Sec. II we give a detailed account of the model we have used and present an overall comparison of the observed Raman spectra with theoretical predictions. In Sec. III phonon dispersion curves are presented which show a pronounced softening of the two modes that become degenerate at the M point. We then list and discuss the eigenvectors and the associated displacements of these soft modes and relate them to the structural differences between the f.e. and p.e. phases.

II. RIGID-ION MODEL FOR PARAELECTRIC GMO

We regard p.e. GMO to be an array of point charges of magnitudes $z_{Gd}e$, $z_{Mo}e$, and $z_O e$, for the gadoliniums, molybdenums, and oxygens, respectively, where e is the absolute magnitude of the electronic charge. These are located at the sites determined by Jeitschko. In Table I we list coordinates for all 34 ions in the unit cell along with the ion label used by Jeitschko and define another label k, where $k = 1, 2, \ldots, 34$. We take $z_{Gd} = +3$ and $z_{Mo} = -2 - 4z_O$, and allow z_O to be an adjustable parameter. We then assume that the ions are held apart by various central short-range forces which act between the molybdenum ions and their four nearest-neighbor oxygen ions, and between the gadolinium ions and their seven nearest-neighbor oxygen ions.

If the static lattice is in equilibrium, then the

TABLE I. Positions of the ions in the p.e. (183 °C) phase as determined by Jeitschko. The coordinates are given with respect to the primitive axes of the p.e. phase and are in units of 10 Å. The origin is shifted by half a lattice vector along the x axis from that used by Jeitschko.

k	x	y	z	Jeitschko's ion designation
1	−0.23108	0.23108	−0.27996	
2	0.23108	−0.23108	−0.27996	Gd(1)
3	0.13857	0.13857	0.27996	
4	−0.13857	−0.13857	0.27996	
5	−0.21689	0.21689	0.38087	
6	0.21689	−0.21689	0.38087	Mo(1)
7	0.15276	0.15276	−0.38087	
8	−0.15276	−0.15276	−0.38087	
9	0.36965	0.0	0.0	MO(3)
10	0.0	0.36965	0.0	
11	−0.22534	0.22534	−0.51269	
12	0.22534	−0.22534	−0.51269	O(1)
13	0.14431	0.14431	0.51269	
14	−0.14431	−0.14431	0.51269	
15	0.09530	−0.09530	0.33173	
16	−0.09530	0.09530	0.33173	O(3)
17	−0.27435	−0.27435	−0.33173	
18	0.27435	0.27435	−0.33173	
19	0.20412	−0.00126	−0.31957	
20	−0.20412	0.00126	−0.31957	
21	−0.36839	−0.16553	0.31957	
22	0.36839	0.16553	0.31957	O(5)
23	−0.00126	0.20412	−0.31957	
24	0.00126	−0.20412	−0.31957	
25	0.16553	0.36839	0.31957	
26	−0.16553	−0.36839	0.31957	
27	0.23266	0.02905	0.10190	
28	−0.23266	−0.02905	0.10190	
29	0.34060	−0.13699	−0.10190	
30	−0.34060	0.13699	−0.10190	O(9)
31	0.02905	0.23266	0.10190	
32	−0.02905	−0.23266	0.10190	
33	−0.13699	0.34060	−0.10190	
34	0.13699	−0.34060	−0.10190	

net force on any sublattice must be zero, and the macroscopic stress due to the short-range forces must cancel that produced by the Coulomb forces which tend to collapse the structure. To set the crystal in static equilibrium the short-range forces must be chosen to satisfy these constraints. Explicit expressions for these static equilibrium conditions are given by Boyer and Hardy[14] for a general rigid-ion crystal. For our model of p.e. GMO we have eight force constants to be determined from these conditions. These are the first derivatives of the short-range interatomic potential between the following ion pairs (we used Jeitschko's notation; see Table I): Mo(3)-O(9); Mo(1)-O(5); Mo(1)-O(1); Mo(1)-O(3); Gd(1)-O(9); Gd(1)-O(1); Gd(1)-O(5); and Gd(1)-O(3).

Unfortunately, this procedure gives 16 linearly independent equilibrium conditions from which these eight force constants have to be determined; 14 are obtained from the sublattice equilibrium conditions and two from the requirements that the macroscopic stresses be zero. Of the 14 sublattice equilibrium conditions, two are provided by Gd(1), two by Mo(1), two by O(1), two by O(3), three by O(5), and three by O(9).

The values of the Coulomb forces $F_\alpha(k)$ obtained using $z_O = -1.25$ are listed in Table II. The reason for using this value for the oxygen charge is discussed below. From the values in Table II it is clear that the Coulomb forces on the oxygens are considerably larger than those on the Gd(1) and Mo(1) ions. The force on the Mo(3) ions is automatically zero. (This is because these ions are at the origin of the $\bar{4}$ operation.) Thus, we only require that the short-range forces cancel, or approximately cancel, the Coulomb forces on the oxygen ions. We also neglect the conditions for zero macroscopic stress and assume the existence of whatever applied stress is necessary to maintain the experimentally determined lattice constants.

From our restrictions on the range of the short-range interactions, we find that the O(1), O(5), and O(9) ions each experience two short-range forces. For the O(3) ions there are three short-range forces, two due to Gd(1) ions, and one due to a Mo(1). However, the two Gd bonds are equivalent and all three bonds lie in the same plane. Furthermore, the Coulomb forces on the O(1) and O(3) ions lie exactly in the plane of the short-range forces and therefore these can be determined so as to cancel these Coulomb forces on the oxygens exactly. The Coulomb forces on the O(5) and O(9) ions lie, to a good approximation, in the plane of the short-range forces. (The component normal to the plane is ~3–4% of the total force in each case.) Thus, we determine the short-range forces acting on these ions by requiring that they cancel the components of the Coulomb force lying in the plane of the short-range forces.

TABLE II. Coulomb force $F_\alpha(k)$ on the ions of the p.e. phase with $z_O = -1.25$. The components are directed along the primitive axes of the p.e. phase, and are given in units such that the charge of the electron and the length 10 Å are both unity.

Ion	Coulomb force $\vec{F}(k)$ F_x	F_y	F_z
1	7.007	−7.007	8.404
5	−7.284	7.284	1.020
9	0.0	0.0	0.0
11	2.746	−2.746	−49.489
15	30.596	−30.596	11.600
19	−19.383	43.969	−24.723
27	50.956	2.706	−18.187

The resultant short-range forces are listed in Table III, along with the associated bond lengths, and are plotted as a function of bond length in Fig. 1.

To perform lattice dynamical calculations we also need the second derivatives of the short-range potentials. We have chosen these second derivatives to be the same for all the Mo-O interactions (ϕ''_{Mo}) and also for the Gd-O interactions (ϕ''_{Gd}). The values taken for ϕ''_{Mo} and ϕ''_{Gd} appear in Fig. 1 as the slopes of the plots of ϕ' against bond length. Clearly, ϕ''_{Gd} and ϕ''_{Mo} can have a fairly wide range of values and still be within the limits one would expect from Fig. 1. The final values chosen for ϕ''_{Mo} and ϕ''_{Gd} were determined by fitting to Raman data. The value of the ionic charge, $z_O = -1.25$, was also chosen in this manner. The masses of the ions are $m_{Gd} = 157.0$, $m_{Mo} = 96.0$, and $m_O = 16.0$, in atomic mass units.

In the foregoing material we have described how we obtain all the parameters necessary to construct the dynamical matrix of p.e. GMO; namely, the charges of the ions, the masses of the ions, their precise locations, and the values of the first and second derivatives of all short-range potentials. General expressions for the dynamical matrix of a rigid-ion lattice[15] have been programmed for the computer so that we can treat any structure within the limits of the rigid-ion model given the necessary input parameters such as those listed above. This program was used in our lattice dynamical calculations for p.e. GMO. The eigenvalues were obtained using a subroutine based on the Householder method, which we find is ~10 times more efficient than the Jacobi method.[16]

In Table IV we list the frequencies of the normal modes of zero wave vector with the macroscopic electric field contributions omitted. The nonacoustic portion of this spectrum of frequencies is plotted as a histogram and compared with a se-

TABLE III. First derivatives of the short-range interatomic potential and the associated bond lengths.

Bond	ϕ' (Same units as those in Table II)	Bond length (Å)
Mo(3) – O(9)	−83.44	1.7319
Mo(1) – O(5)	−80.09	1.7354
Mo(1) – O(1)	−63.55	1.7385
Mo(1) – O(3)	−53.09	1.7884
Gd(1) – O(9)	−38.16	2.2924
Gd(1) – O(1)	−13.92	2.3287
Gd(1) – O(5)	−27.64	2.3476
Gd(1) – O(3)	−7.02	2.4341

lected Raman spectrum[17] in Fig. 2. The highest frequencies depend strongly upon ϕ''_{Mo}, thus the value of ϕ''_{Mo} was chosen so that these coincided with the corresponding group of peaks in the Raman spectrum. The values of ϕ''_{Gd} and z_O were chosen to fit the lower end of the frequency spectrum to the Raman spectrum. Specifically, the lowest frequency mode depends upon ϕ''_{Gd} and z_O in the following manner: For any reasonable z_O, i.e., $-2 < z_O < -1$ the lower limit of the frequency spectrum increases with increasing ϕ''_{Gd}, and approaches a limiting value which depends upon z_O. We find that the largest limiting value is obtained using $z_O = -1.25$. For this value of z_O and a reasonable value of ϕ''_{Gd} (cf. Fig. 1) the lowest frequency is that shown in Table IV and is close to the limiting value.

From the results given in Table IV it is clear that our lowest frequency modes are too low, but over all, the correspondence between theory and

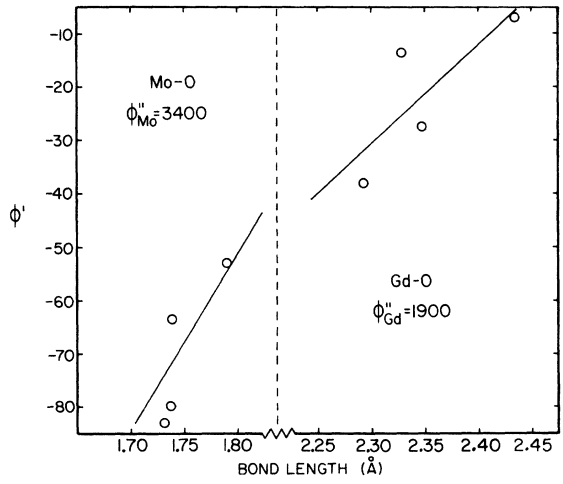

FIG. 1. Plot of the first derivatives of the short-range interatomic potentials ϕ' as a function of bond length. ϕ' is measured in units such that the electronic charge and 10 Å are unity. The slopes of the lines are given by ϕ''_{Mo} and ϕ''_{Gd}.

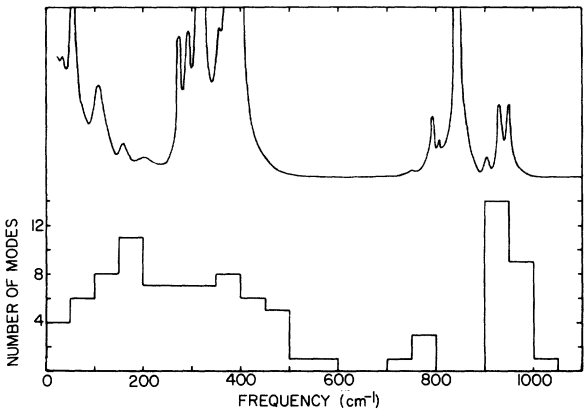

FIG. 2. Histogram of the frequency spectrum of the $\vec{q}=0$ phonons of p.e. GMO compared with the $x(yx)y$ Raman spectrum.

experiment in Fig. 2 is surprisingly good, considering the simplicity of the model that we have used. We believe that the probable cause of our inability to fit the low-frequency end of the spectrum is that we have not included enough short-range interactions to put the crystal in complete static equilibrium.

When the macroscopic electric field contribution to the dynamical matrix is included certain of the degeneracies shown in Table IV are lifted. The resultant splitting depends upon the direction of the wave vector. However, this modification does not affect the correlation shown in Fig. 2. In particular, we find that the lowest frequency mode is unaffected by the electric field contribution.

The comparison in Fig. 2 is not the only one possible. We could also make comparisons with experimental spectra obtained for other scattering

TABLE IV. List of eigenfrequencies of the dynamical matrix at zero wave vector without the macroscopic electric field contribution. Frequencies are in cm^{-1}.

0.0	131.6	224.6	333.2	474.0	937.1
0.0	131.6	236.4	344.7	474.0	941.1
0.0	133.1	240.7	355.1	483.1	942.1
20.5	134.2	240.7	355.1	484.2	944.7
23.4	154.9	249.9	358.3	533.7	944.8
23.4	154.9	278.6	359.7	559.8	944.9
37.8	157.8	278.6	362.4	745.9	944.9
56.5	157.9	280.3	362.4	754.9	957.6
56.5	167.8	288.8	363.1	779.4	963.2
65.2	172.2	288.8	397.3	779.4	966.8
88.0	172.2	294.8	407.1	901.8	966.8
96.0	186.2	295.9	407.1	901.8	972.6
96.0	190.7	308.0	424.6	903.4	977.6
111.1	190.8	309.9	424.6	927.6	984.2
111.1	190.8	314.3	427.8	927.6	984.2
118.5	218.6	314.3	428.9	935.1	998.6
130.4	218.6	323.7	455.2	937.1	1008.3

geometries. However, until we know more about the symmetries of the computed eigenvectors this would be premature. For the present all that we can say is that we do not necessarily expect the Raman spectrum to show all the $\vec{q}=0$ modes and thus the present comparison is only semiquantitative.

III. SOFT-ZONE-EDGE MODES

Using the model described in detail in Sec. II, we have computed the phonon dispersion curves for modes propagating along the [110] direction in p.e. GMO. The results of these calculations are shown in Fig. 3.

The important feature of Fig. 3 is the occurrence of two soft degenerate modes at the zone edge (M point); in fact, for these modes our model lattice is unstable. Also present is an acoustic instability, but this instability is not as prominent as that of the two zone-edge modes. This acoustic instability is probably due to the fact that the frequency of the lowest zone center mode is too small. This can result in acoustic instability.[18] As was mentioned above, we believe this difficulty is probably due to our failure to satisfy the static equilibrium conditions exactly.

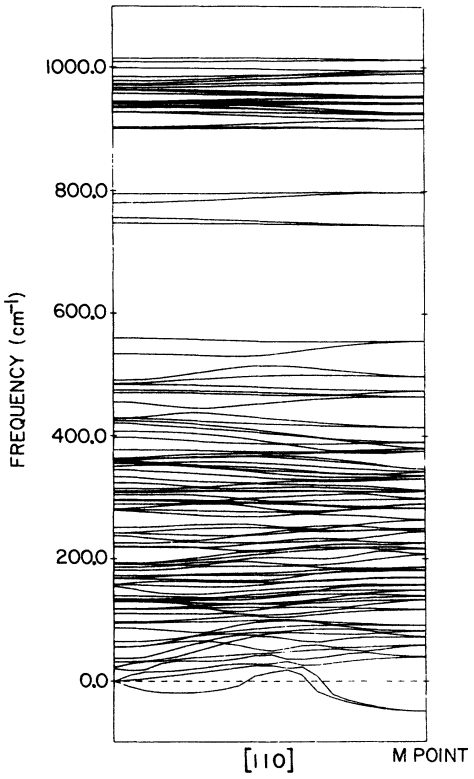

FIG. 3. Phonon dispersion curves for p.e. GMO, with wave vector along the [110] direction. The "curves" were plotted by computer, and therefore, their appearance at points of intersection may be a little misleading. Imaginary frequencies are plotted here as negative real.

The eigenvectors for the soft doubly degenerate $(\frac{1}{2},\frac{1}{2},0)$ modes were obtained as follows. A matrix $G=[D-\omega_s^2(1+\delta)I]^{-1}$ was constructed from the dynamical matrix D. I is the unit matrix, ω_s^2 is the lowest eigenvalue of D (i.e., the square of the soft-mode frequency), and δ is a small positive number. One can easily show that if E_s is an eigenvector of D associated with the eigenvalue ω_s^2, then E_s is also an eigenvector of G with eigenvalue $1/-\omega_s^2\delta$. Since δ is small, $1/-\omega_s^2\delta$ is much larger than the other eigenvalues of G, and for any vector X, the vector G^nX will converge rapidly, as n increases, to an eigenvector associated with this largest eigenvalue.[19]

Since the two soft modes are degenerate, the vector G^nX may lie anywhere in a two-dimensional "plane" in the hyperspace of eigenvectors. However, by starting with two different vectors X and X', we obtain linearly independent eigenvectors, G^nX and G^nX', and from these an orthonormal basis can be constructed. Two such orthonormal eigenvectors, denoted by $S_\alpha(k,j)$ with $j=1$ or 2, are listed in Table V.

The displacement of the ion (l,k) due to all the crystal vibrations is given by

$$u_\alpha(l,k)\propto\frac{1}{(m_k)^{1/2}}\sum_{j\vec{q}}e_\alpha(k,j|\vec{q})\,Q(j|\vec{q})\times e^{i[\vec{q}\cdot\vec{x}(l,k)+\Delta(j|\vec{q})]}\,, \quad (1)$$

where $e_\alpha(k,j|\vec{q})$ is the jth eigenvector of the dynamical matrix, $D_{\alpha\beta}(\vec{q},k,k')$ for wave vector $\vec{q}$, $Q(j|\vec{q})$ is the complex normal coordinate of the mode $(j|\vec{q})$, $\vec{x}(l,k)$ is the position of the (l,k) ion, and m_k is the mass of the kth ion. The factor $e^{i\Delta(j|\vec{q})}$ accounts for the fact that all the components $e_\alpha(k,j|\vec{q})$ contain an arbitrary phase factor. It is important to note that one must be careful to express the displacements in a manner consistent with the definition of the dynamical matrix [see discussion following Eq. (38.29) of Ref. 15]. In our calculations we included the factor $e^{-i\vec{q}\cdot[\vec{x}(k)-\vec{x}(k')]}$ in the definition of $D_{\alpha\beta}(\vec{q},k,k')$, and for this definition the displacements are given correctly by Eq. (1).

Combining the contributions due to the $(\frac{1}{2},\frac{1}{2},0)$ and the $-(\frac{1}{2},\frac{1}{2},0)$ modes, the displacements due to the jth soft mode are given by

$$\xi_\alpha(l,k|j)\propto\frac{1}{(m_k)^{1/2}}\,[S_\alpha(k,j)Q(j)\,e^{i[\beta(l,k)+\Delta(j)]}+S_\alpha^*(k,j)\,Q^*(j)\,e^{-i[\beta(l,k)+\Delta(j)]}]\,, \quad (2)$$

where $\beta(l,k)=\vec{q}_0\cdot\vec{x}(l,k)$, $\vec{q}_0=(\pi/a)(1,1,0)$, a is the unit cell side in the xy plane, and $S_\alpha(k,j)$ are the eigenvector components.

The normal coordinates may be written $Q(j)$

TABLE V. The orthonormal sets of soft-mode eigenvectors $S_\alpha(k,j)$: $j=1$ and $j=2$, written in the polar form $S_\alpha(k,j)=R_\alpha(k,j)\exp[-i\theta_\alpha(k,j)]$, where $\theta_\alpha(k,j)$ is given in degrees.

k	$R_x(k,1)$	$\theta_x(k,1)$	$R_y(k,1)$	$\theta_y(k,1)$	$R_z(k,1)$	$\theta_z(k,1)$	$R_x(k,2)$	$\theta_x(k,2)$	$R_y(k,2)$	$\theta_y(k,2)$	$R_z(k,2)$	$\theta_z(k,2)$
1	0.023 44	119.808	0.023 44	119.805	0.0	0.0	0.025 65	124.211	0.025 65	124.208	0.0	0.0
2	0.023 44	299.804	0.023 44	299.808	0.0	0.0	0.025 65	304.206	0.025 65	304.211	0.0	0.0
3	0.011 61	236.745	0.011 61	56.745	0.0	0.0	0.005 13	107.372	0.005 13	287.372	0.0	0.0
4	0.011 61	281.792	0.011 61	101.787	0.0	0.0	0.005 14	152.418	0.005 14	332.417	0.0	0.0
5	0.076 98	341.662	0.076 98	341.663	0.0	0.0	0.034 57	244.871	0.034 57	244.871	0.0	0.0
6	0.076 98	161.663	0.076 98	161.662	0.0	0.0	0.034 57	64.872	0.034 57	64.871	0.0	0.0
7	0.132 19	192.007	0.132 19	12.007	0.0	0.0	0.149 01	119.718	0.149 01	19.718	0.0	0.0
8	0.132 19	223.234	0.132 19	43.234	0.0	0.0	0.149 01	230.945	0.149 01	50.945	0.0	0.0
9	0.028 44	315.547	0.083 56	37.871	0.0	0.0	0.036 15	60.217	0.080 53	29.374	0.0	0.0
10	0.083 56	217.871	0.028 44	135.547	0.0	0.0	0.080 53	209.374	0.036 15	240.217	0.0	0.0
11	0.033 29	107.149	0.033 29	107.147	0.0	0.0	0.042 17	129.959	0.042 17	129.958	0.0	0.0
12	0.033 29	287.146	0.033 29	287.149	0.0	0.0	0.042 17	309.958	0.042 17	309.958	0.0	0.0
13	0.035 03	214.676	0.035 03	34.676	0.0	0.0	0.023 61	173.526	0.023 61	353.526	0.0	0.0
14	0.035 03	254.136	0.035 03	74.136	0.0	0.0	0.023 61	212.985	0.023 61	32.983	0.0	0.0
15	0.004 03	340.621	0.004 03	340.621	0.0	0.0	0.001 84	248.078	0.001 84	248.078	0.0	0.0
16	0.004 03	160.621	0.004 03	160.621	0.0	0.0	0.001 84	68.078	0.001 84	68.078	0.0	0.0
17	0.006 75	343.662	0.006 75	163.662	0.0	0.0	0.007 65	351.913	0.007 64	171.913	0.0	0.0
18	0.006 75	70.854	0.006 75	250.854	0.0	0.0	0.007 65	79.108	0.007 65	259.107	0.0	0.0
19	0.368 97	164.047	0.028 24	163.488	0.051 52	335.622	0.431 66	176.147	0.033 26	176.403	0.065 80	359.710
20	0.368 97	245.264	0.028 24	244.706	0.051 52	236.837	0.431 66	257.364	0.033 26	257.622	0.065 80	260.926
21	0.020 76	23.411	0.262 02	204.482	0.056 38	193.612	0.011 06	317.237	0.135 85	134.774	0.038 77	154.349
22	0.020 76	103.398	0.262 02	284.472	0.056 38	93.605	0.011 06	37.223	0.135 85	214.765	0.038 77	54.342
23	0.028 24	343.486	0.368 97	344.047	0.051 52	155.622	0.033 26	356.404	0.431 66	356.147	0.065 80	179.710
24	0.028 24	64.705	0.368 97	65.264	0.051 52	56.837	0.033 26	77.622	0.431 66	77.364	0.065 80	80.926
25	0.262 02	104.472	0.020 76	283.398	0.056 38	273.605	0.135 85	34.765	0.011 06	217.223	0.038 77	234.342
26	0.262 02	24.482	0.020 76	203.412	0.056 38	13.612	0.135 85	314.774	0.011 06	137.237	0.038 77	334.349
27	0.026 22	247.656	0.011 97	41.135	0.019 92	237.841	0.015 93	66.953	0.005 79	321.009	0.009 49	88.849
28	0.026 22	300.218	0.011 97	93.717	0.019 93	110.414	0.015 93	119.514	0.005 79	13.588	0.009 49	321.415
29	0.018 41	345.591	0.065 55	352.258	0.043 71	170.478	0.021 18	355.688	0.068 78	352.195	0.047 09	173.192
30	0.018 41	66.443	0.065 55	73.110	0.043 71	71.331	0.021 18	76.543	0.068 78	73.047	0.047 09	74.046
31	0.011 97	221.135	0.026 22	67.656	0.019 92	57.843	0.005 79	141.014	0.015 93	246.953	0.009 49	268.849
32	0.011 97	273.717	0.026 22	120.218	0.019 92	290.415	0.005 79	193.588	0.015 93	299.514	0.009 49	141.412
33	0.065 55	172.258	0.018 41	165.592	0.043 71	350.478	0.068 78	172.195	0.021 18	175.688	0.047 09	353.192
34	0.065 55	253.110	0.018 41	246.443	0.043 81	251.331	0.068 78	253.047	0.021 18	256.542	0.047 09	254.045

$= Q_1(j) + iQ_2(j)$, where $Q_1(j)$ and $Q_2(j)$ are solutions of the harmonic oscillator equation. Thus, if we set $Q(j) \propto 1+i$, Eq. (2) may be written

$$\xi_\alpha(l,k\,|\,j) \propto \frac{R_\alpha(k,j)}{(m_k)^{1/2}} \{\cos[\beta(l,k) - \theta_\alpha(k,j) + \Delta(j)] - \sin[\beta(l,k) - \theta_\alpha(k,j) + \Delta(j)]\}, \quad (3)$$

where we have expressed the eigenvectors in the polar form $S_\alpha(k,j) = R_\alpha(k,j)\, e^{-i\theta_\alpha(k,j)}$, as they are listed in Table V.

The soft-mode theory of displacive phase transitions hypothesizes that at the transition the displacements associated with the soft mode (or modes) are "frozen" or "condensed" into the phase of lower symmetry. That is, the difference between the structure of the two phases corresponds to the displacements associated with the soft modes in the higher-symmetry phase.

The structure of f.e. GMO has been determined by Jeitschko.[5,6] He concludes that ferroelectric switching may be visualized as an application of the $\bar{4}$ operation, which was a symmetry operation of the high-temperature phase.[6] Thus, we can determine the positions of the ions in the ferroelectrically switched phase from Jeitschko's values by performing a rotation of 90° about the $x = \frac{1}{4}$, $y = \frac{1}{4}$ axis followed by a reflection in the $z = 0$ plane.

The $\bar{4}$ operation may be applied n times, where $n = 0, 1, 2$, or 3, to obtain four different sets of ion coordinates. Hence, when one subtracts from these, the coordinates of the ions in the p.e. phase one obtains four different sets of displacements denoted by $\vec{w}(l,k\,|\,n)$, to be interpreted as arising from "frozen in" soft modes. In Table VI we list the displacements associated with the structural difference between the two phases for the $k = 19$ and $k = 21$ ions. These displacements were computed for zero macroscopic strain, i.e., the lattice constants of the f.e. phase were taken to be $a = b = 10.4554$ Å and $c = 10.6700$ Å, which correspond to those of the p.e. phase, instead of those of the room-temperature phase.

An important feature of the displacements $\vec{w}(l,k\,|\,n)$ is that those associated with an even (or odd) number of applications of the $\bar{4}$ operation differ primarily only in their sign; i.e., $\vec{w}(l,k\,|\,n) \cong -\vec{w}(l,k\,|\,n+2)$.

For example, using the data given in Table VI, we find that the angle between $\vec{w}(0,19\,|\,0)$ and $\vec{w}(0,19\,|\,2)$ is 175.1° and the angle between $\vec{w}(0,19\,|\,1)$ and $\vec{w}(0,19\,|\,3)$ is 174.2°, while the lengths of these vectors are, respectively, 0.3435, 0.3801, 0.3483, and 0.3453 Å for $n = 0, 2, 1$, and 3. This approximation is not as good for some of the other ions which have smaller displacements, and is poorest for the O(9) ions. For $k = 27$, which refers to an O(9) ion, the corresponding angles and lengths are 167.8°, 155.3°, 0.1444, 0.0938, 0.1355, and 0.0906 Å. Because of the fact that $\vec{w}(l,k\,|\,n) \cong -\vec{w}(l,k\,|\,n+2)$, we characterize the "frozen in" displacements by $\vec{\eta}(l,k) = \frac{1}{2}[\vec{w}(l,k\,|\,0) - \vec{w}(l,k\,|\,2)]$ and $\vec{\eta}'(l,k) = \frac{1}{2}[\vec{w}(l,k\,|\,1) - \vec{w}(l,k\,|\,3)]$ and their negative counterparts.

Equation (3) gives the displacements due to one or other of a pair of orthogonal eigenvectors. However, these are still arbitrary and we now define a new pair of vectors:

$$\zeta_\alpha(l,k) = a_1 \xi_\alpha(l,k\,|\,1) + a_2 \xi_\alpha(l,k\,|\,2) \quad (4)$$

and its orthogonal counterpart

$$\zeta'_\alpha(l,k) = -a_2 \xi_\alpha(l,k\,|\,1) + a_1 \xi_\alpha(l,k\,|\,2). \quad (5)$$

We are now free to *choose* the coefficients a_1, a_2 and the phase angles $\Delta(1)$, $\Delta(2)$, so that $\zeta_\alpha(l,k)$ and $\zeta'_\alpha(l,k)$ fit the largest components of the displacements $\vec{\eta}(l,k)$ and $\vec{\eta}'(l,k)$, for the O(5) ions. Specifically, if we take $a_1 = 8.5093$ Å, $a_2 = -1.0088$ Å, $\Delta(1) = -2.734°$, and $\Delta(2) = 5.021°$, then $\zeta_x(l,19) = \eta_x(l,19)$, $\zeta'_x(l,19) = \eta'_x(l,19)$, $\zeta_y(l,21) = \eta_y(l,21)$, and $\zeta'_y(l,21) = \eta'_y(l,21)$. The displacements $\vec{\zeta}(0,k)$ and $\vec{\zeta}'(0,k)$ obtained using the parameters given above, together with the corresponding displacements $\vec{\eta}(0,k)$ and $\vec{\eta}'(0,k)$, which characterize the difference in the structure of the f.e. and p.e. phases, are listed in Table VII for all values of k. For the other lattice points $\vec{\zeta}(l,k) = (-1)(l_x + l_y) \times \vec{\zeta}(0,k)$ with similar expressions for $\vec{\zeta}'(l,k)$, $\vec{\eta}(l,k)$, and $\vec{\eta}'(l,k)$.

The differences between the calculated and measured displacements are displayed pictorially in

TABLE VI. Displacements of the $k = 19$ and $k = 21$ sublattice ions obtained from the structural differences between the f.e. phase after n applications of the 4 operation and the p.e. phase. The values listed are those obtained using lattice constants $a = b = 10.4554$ Å and $c = 10.6700$ Å for the f.e. phase. The axes are those of the p.e. phase. Displacements are in Å.

	$\vec{w}(0,19\,\|\,n)$			$\vec{w}(0,21\,\|\,n)$		
n	x	y	z	x	y	z
0	0.2772	−0.0037	−0.2027	0.0384	0.3327	0.0843
1	0.3327	−0.0384	−0.0843	−0.0148	−0.3238	−0.1985
2	−0.3238	0.0148	0.1985	−0.0178	−0.3430	−0.0577
3	−0.3430	0.0178	0.0577	0.0037	0.2772	0.2027

TABLE VII. The displacements $\zeta(0,k)$ and $\zeta'(0,k)$ due to the two soft M-point modes compared with those [$\eta(0,k)$ and $\eta'(0,k)$] obtained from the difference in the structure of the f.e. and p.e. phases of GMO. The displacements depend upon the cell index l through the factor $(-1)^{(l_x+l_y)}$. The components are along the primitive axes of the p.e. phase and are listed in Å.

	$\zeta(0,k)$			$\eta(0,k)$			$\zeta'(0,k)$			$\eta'(0,k)$		
k	x	y	z	x	y	y	x	y	z	x	y	z
1	0.0041	0.0041	0.0	0.0343	0.0343	0.0	0.0073	0.0073	0.0	0.0519	0.0519	0.0
2	−0.0041	−0.0041	0.0	−0.0343	−0.0343	0.0	−0.0073	−0.0073	0.0	−0.0519	−0.0519	0.0
3	−0.0073	0.0073	0.0	−0.0519	0.0519	0.0	0.0041	−0.0041	0.0	0.0343	−0.0343	0.0
4	0.0073	−0.0073	0.0	0.0519	−0.0519	0.0	−0.0041	0.0041	0.0	−0.0343	0.0343	0.0
5	0.0513	0.0513	0.0	0.0815	0.0815	0.0	−0.0355	−0.0355	0.0	−0.0214	−0.0214	0.0
6	−0.0513	−0.0513	0.0	−0.0815	−0.0815	0.0	0.0355	0.0355	0.0	0.0214	0.0214	0.0
7	0.0355	−0.0355	0.0	0.0214	−0.0214	0.0	0.0513	−0.0513	0.0	0.0815	−0.0815	0.0
8	−0.0355	0.0355	0.0	−0.0214	0.0214	0.0	−0.0513	0.0513	0.0	−0.0815	0.0815	0.0
9	−0.0358	−0.0037	0.0	−0.1098	0.0041	0.0	0.0037	−0.0358	0.0	−0.0041	−0.1098	0.0
10	0.0037	0.0358	0.0	−0.0041	0.1098	0.0	0.0358	−0.0037	0.0	0.1098	0.0041	0.0
11	0.0399	0.0399	0.0	0.0872	0.0872	0.0	0.0272	0.0272	0.0	0.1471	0.1471	0.0
12	−0.0399	−0.0399	0.0	−0.0872	−0.0872	0.0	−0.0272	−0.0272	0.0	−0.1471	−0.1471	0.0
13	−0.0272	0.0272	0.0	−0.1471	0.1471	0.0	0.0399	−0.0399	0.0	0.0872	−0.0872	0.0
14	0.0272	−0.0272	0.0	0.1471	−0.1471	0.0	−0.0399	0.0399	0.0	−0.0872	0.0872	0.0
15	0.0064	0.0064	0.0	0.0510	0.0510	0.0	−0.0046	−0.0046	0.0	−0.0444	−0.0444	0.0
16	−0.0064	−0.0064	0.0	−0.0510	−0.0510	0.0	0.0046	0.0046	0.0	0.0444	0.0444	0.0
17	0.0046	−0.0046	0.0	0.0444	−0.0444	0.0	0.0064	−0.0064	0.0	0.0510	−0.0510	0.0
18	−0.0046	0.0046	0.0	−0.0444	0.0444	0.0	−0.0064	0.0064	0.0	−0.0510	0.0510	0.0
19	0.3005[a]	0.0238	−0.0641	0.3005	−0.0092	−0.2006	0.3378[a]	0.0257	−0.0414	0.3378	−0.0281	−0.0710
20	−0.3005	−0.0238	−0.0641	−0.3005	0.0092	−0.2006	−0.3378	−0.0257	−0.0414	−0.3378	0.0281	−0.0710
21	−0.0257	0.3378[a]	0.0414	0.0281	0.3378	0.0710	0.0238	−0.3005[a]	−0.0641	−0.0092	−0.3005	−0.2006
22	0.0257	−0.3378	0.0414	−0.0281	−0.3378	0.0710	−0.0238	0.3005	−0.0641	0.0092	0.3005	−0.2006
23	−0.0238	−0.3005	0.0641	0.0092	−0.3005	0.2006	−0.0257	−0.3378	0.0414	0.0281	−0.3378	0.0710
24	0.0238	0.3005	0.0641	−0.0092	0.3005	0.2006	0.0257	0.3378	0.0414	−0.0281	0.3378	0.0710
25	0.3378	−0.0257	−0.0414	0.3378	0.0281	−0.0710	−0.3005	0.0238	0.0641	−0.3005	−0.0092	0.2006
26	−0.3378	0.0257	−0.0414	−0.3378	−0.0281	−0.0710	0.3005	−0.0238	0.0641	0.3005	0.0092	0.2006
27	−0.0658	0.0171	−0.0431	−0.1090	0.0388	−0.0251	0.0255	−0.0137	0.0212	0.0159	−0.1061	0.0267
28	0.0658	−0.0172	−0.0431	0.1090	−0.0388	−0.0251	−0.0255	0.0137	0.0212	−0.0159	0.1061	0.0267
29	−0.0137	−0.0255	0.0212	−0.1061	−0.0159	0.0267	−0.0172	−0.0658	0.0431	−0.0388	−0.1090	0.0251
30	0.0137	0.0255	0.0212	0.1061	0.0159	0.0267	0.0172	0.0658	0.0431	0.0388	0.1090	0.0251
31	−0.0171	0.0658	0.0431	−0.0388	0.1090	0.0251	0.0137	−0.0255	−0.0212	0.1061	−0.0159	−0.0267
32	0.0172	−0.0658	0.0431	0.0388	−0.1090	0.0251	−0.0137	0.0255	−0.0212	−0.1061	0.0159	−0.0267
33	0.0255	0.0137	−0.0212	0.0159	0.1061	−0.0267	0.0658	0.0172	−0.0431	0.1090	0.0388	−0.0251
34	−0.0255	−0.0137	−0.0212	−0.0159	−0.1061	−0.0267	−0.0658	−0.0172	−0.0431	−0.1090	−0.0388	−0.0251

[a]Fitted.

Fig. 4. There are 13 nonequivalent displacement differences. The measured displacements are denoted by solid vertical arrows with length proportional to the magnitude of the displacement. The lengths of the dashed arrows denote the magnitudes of the calculated displacements while their directions show the directional deviation from the measured values.

There is clearly a correlation between our calculated soft-mode displacements and those obtained from the structures of the two phases. There are some discrepancies; particularly in that the magnitudes of the calculated displacements, other than those which we fit, are too small. On the other hand, one does not expect the soft-mode displacements to be frozen into the crystal exactly, owing to the higher-order effects that are significant at the transition and which are responsible for the onset of the permanent polarization. Also the use of our oversimplified model may be causing some of the discrepancies.

Perhaps the most important factor which spoils the correlation is the fact that the f. e. structure, which we have used to determine $\vec{\eta}(l,k)$ and $\vec{\eta}'(l,k)$, was determined at room temperature. Jeitschko has shown that the structure changes continuously with temperature from room temperature to just below 159 °C and that about half the change in structure occurs over this temperature range.[6] For a better comparison, we really need the structure of f. e. GMO at a temperature just below 159 °C. On the whole however, we believe the present correlation is quite good and provides new insight into the nature of the transition and the formation and switching of f. e. domains.[14]

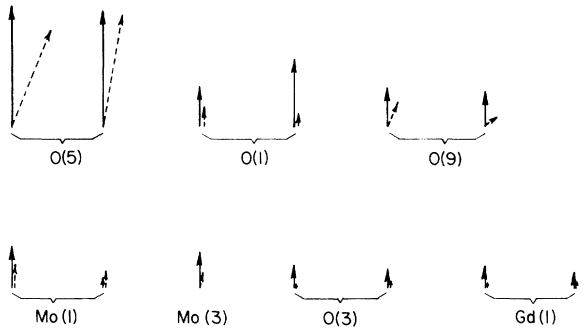

FIG. 4. Comparison of the measured displacements (solid arrows) with the computed values (dashed arrows) given in Table VII. The solid arrows are assigned a vertical direction and the lengths and angular deviations are drawn to scale.

ACKNOWLEDGMENTS

We are very grateful to Dr. S. C. Abrahams, Dr. W. Jeitschko, and Dr. J. D. Axe and their coauthors for preprints of their work. In particular, the present work has made extensive use of Dr. Jeitschko's results.

*Research sponsored by the Air Force Office of Scientific Research, Air Force Systems Command, USAF, under Grant No. AFOSR 70-1926. The U.S. Government is authorized to reproduce and distribute reprints for Governmental purposes notwithstanding any copyright notation hereon.

†Present address: Solid State and Materials Laboratory, Princeton University, Princeton, N.J.

[1]H. J. Borchardt and P. E. Bierstedt, Appl. Phys. Lett. **8**, 50 (1966).

[2]L. E. Cross, A. Fouskova, and S. E. Cummins, Phys. Rev. Lett. **21**, 812 (1968).

[3]S. E. Cummins, Ferroelectrics **1**, 11 (1970).

[4]E. T. Keve, S. C. Abrahams, and J. L. Bernstein, J. Chem. Phys. **54**, 3185 (1971).

[5]W. Jeitschko, Naturwissenschaften **57**, 544 (1970).

[6]W. Jeitschko, Acta Crystallogr. B **28**, 60 (1972).

[7]E. Pytte, Solid State Commun. **8**, 2101 (1970).

[8]A. P. Levanyuk and D. G. Sannikov, Fiz. Tverd. Tela **12**, 2997 (1970) [Sov. Phys.-Solid State **12**, 2418 (1971)].

[9]K. Aizu, J. Phys. Soc. Jap. **31**, 802 (1971).

[10]J. D. Axe, B. Dorner, and G. Shirane, Phys. Rev. Lett. **26**, 519 (1971).

[11]B. Dorner, J. D. Axe, and G. Shirane, Phys. Rev. B **6**, 1950 (1972).

[12]A group theoretical analysis of the M-point vibrations has also been worked out by J. Petzelt and V. Dvorak, Phys. Status Solidi B **46**, 413 (1971).

[13]L. L. Boyer and J. R. Hardy, Solid State Commun. **11**, 55 (1972). Such domains have recently been observed [J. R. Barkley and W. Jeitschko, J. Appl. Phys. **44**, 938 (1973)].

[14]L. L. Boyer and J. R. Hardy, Phys. Rev. B (to be published).

[15]M. Born and K. Huang, *Dynamical Theory of Crystal Lattices* (Oxford U. P., London, 1954).

[16]For a good discussion of these methods see, Forman S. Acton, *Numerical Methods that Work* (Harper and Row, New York, 1970), Chap. 8.

[17]J. R. Hardy, F. G. Ullman, and L. L. Boyer, AFOSR Interim Scientific Report No. AFOSR-TR-71-2138, Chap. IV, Sec. E, August, 1971 (unpublished).

[18]P. B. Miller and J. D. Axe, Phys. Rev. **163**, 924 (1967); also Chap. III of Ref. 17.

[19]Strictly speaking, if one were sufficiently unlucky to choose x with only a very small component in the space of the required eigenvector, then the convergence would be poor.